Electron Microscopic Study of Intergrowth of MFI and MEL: Crystal Faults in B-MEL†

Tetsu Ohsuna,*,‡ Osamu Terasaki,§ Yumi Nakagawa,|| Stacey I. Zones,|| and Kenji Hiraga‡

Institute for Materials Research, Tohoku University, Sendai 980-77, Japan, Department of Physics, Graduate School of Science and Interdisciplinary Research Center, Tohoku University, Sendai 980-77, Japan, and Chevron Research and Technology Company, 100 Chevron Way, Richmond, California

Received: April 29, 1997⊗

Recently, a pure MEL type silica zeolite was successfully synthesized by one of the authors. Boron atoms were incorporated into its framework structure by using similar synthesis conditions with gels containing boron in an effort to confer catalytic activity. The nature of crystal faults in the borosilicate-MEL zeolite (B-MEL) was studied using transmission and scanning electron microscopy (TEM and SEM). Electron diffraction (ED) patterns show characteristic diffuse streaks along the [100] and [010] directions. From the analyses of both the diffuse streaks in ED patterns and high-resolution electron microscopy (HREM) images, it was determined that the framework structure of the B-MEL crystal has many planar faults that are parallel to the (100) and (010) planes. The local structure of the planar faults can be interpreted by the intergrowth of the MFI type structure, and a model of the growth process for the B-MEL is speculated from the results.

Introduction

ZSM-5 (MFI) is one of the most useful zeolites for the petrochemical industry, and its synthesis, catalytic properties, and crystal structure have been studied for over 20 years.[1] MFI is regarded as one end-member of polytypes of the pentasil zeolite family. The other end-member is ZSM-11 (MEL) zeolite, which has a framework structure showing the highest symmetry in the polytypes.[2] Framework structures of these two zeolites are closely related to each other. Their framework structures can be described using a stacking manner of pentasil sheets, so the possibility of intergrowths between them was suggested from the beginning. Sir John M. Thomas and his group succeeded in producing high-resolution electron microscope (HREM) images of zeolites. They have proved an advantage of using HREM to study various kinds of intergrowths and recurrent twins by showing the fine structures of FAU/EMT and MTT/TON.[3−5] Extensive studies have been reported by Millward, Ramdas, and Thomas[6] and by Terasaki, Thomas, Millward, and Watanabe[7] to find and characterize the intergrowths and to detect different symmetry elements between MFI and MEL by TEM. Intergrowth crystals of MEL/MFI are frequently synthesized under several synthesis conditions.[8] To control the catalytic properties of zeolites, synthesis with elements other than Si and Al atoms has been often performed.[9−12] Such modifications of the MFI synthesis results in various intergrowth crystals, as reported by Perego, Cesari, and Allegra.[13] They discussed the intergrowth structure of a borosilicate based on the MFI structure by powder X-ray diffraction using the sheet-stacking model. Certainly, the intergrowth close to the MFI structure can be explained by the manner of sheet stacking. However, it is difficult to explain intergrowths close to the MEL structure because, owing to its symmetry, there are two equivalent and independent directions with respect to the stacking direction in the MEL crystal. To investigate such an intergrowth structure, analysis of a powder X-ray diffraction pattern is too complicated and indirect, whereas high-resolution electron microscopy (HREM) and electron diffraction (ED) are the most useful and direct methods. Even from micrometer-sized areas, diffraction patterns of single crystals can be obtained by a selected area ED method, and stacking manners of the zeolitic framework in real space can be directly read from HREM images.[14]

Recently, we have reported the synthesis of pure all-silica MEL crystals and the structural analysis in an HREM study.[15−16] We have also synthesized a borosilicate MEL (B-MEL) using MEL as a seed crystal and found crystal faults in the crystal by HREM and ED observations. In this paper, the details of the nature of the faults are reported.

Structural Representation of MFI and MEL

To simplify the discussion of the framework structures of both MFI and MEL, new notations are introduced as below. The MFI and MEL framework structures have been described by stacking manners of pentasil sheets. Figure 1a shows a perspective view of the sheet. The MEL structure is formed from successive sheets, which are connected each other with a mirror relation, along the [100] direction, whereas MFI is formed by an inversion relation (Figure 1b). These relations can be directly seen in HREM images, as shown in Figure 1c (inserted rectangles correspond to a part of the sheet in Figure 1b). The pentasil sheet can be divided into two different parts, which are related to each other by mirror symmetry (Figure 2a). In this paper, those are named "pentasil chains". These chains are introduced to describe intergrowth structures. The pentasil chains have a spiral form, so the two chains are differentiated by their chirality and identified as L (left spiral) and R (right spiral). Projected framework structures of MEL and MFI along the [001] direction are described with the L and R notations. L_I and L_{II} have the same framework structure, but L_{II} is rotated at 90° from L_I around the chain direction, and R_I and R_{II} have the same relationship. The first neighbors of the R chain must be L and vice versa in both the MFI and MEL structures, as clearly seen in Figure 2b. Along the [001] direction, L_I and R_{II}, and L_{II} and R_I give the same projected structures, which are called A chain and B chain, respectively (Figure 2a). In the projected framework structures of MEL and MFI along the [001] direction, the unit cells of MEL and MFI consist of four chains of two A and two B, as shown in Figure 2b. Corresponding HREM

† Dedicated to the 65th birthday of Sir John Meurig Thomas.
‡ Institute for Materials Research, Tohoku University.
§ Graduate School of Science and Interdisciplinary Research Center, Tohoku University.
|| Chevron Research and Technology Company.
⊗ Abstract published in *Advance ACS Abstracts,* October 15, 1997.

S1089-5647(97)01448-X CCC: $14.00

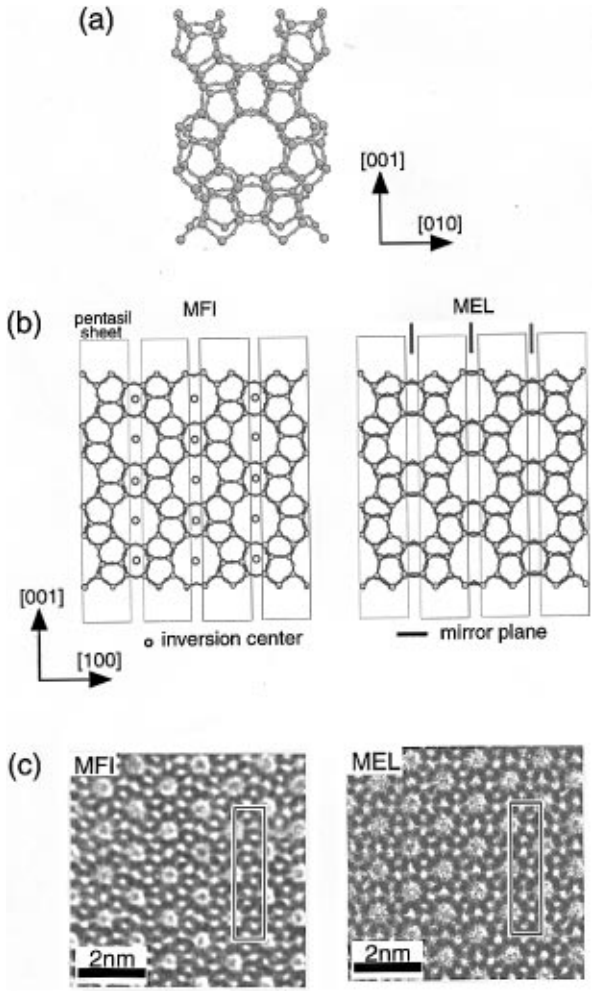

Figure 1. Schematic diagrams of (a) framework of pentasil sheet and (b) projected framework structures of MFI and MEL along the [010] direction and and (c) corresponding HREM images of MFI and MEL. Rectangles inserted in (c) show a part of the pentasil sheet corresponding to those in (b).

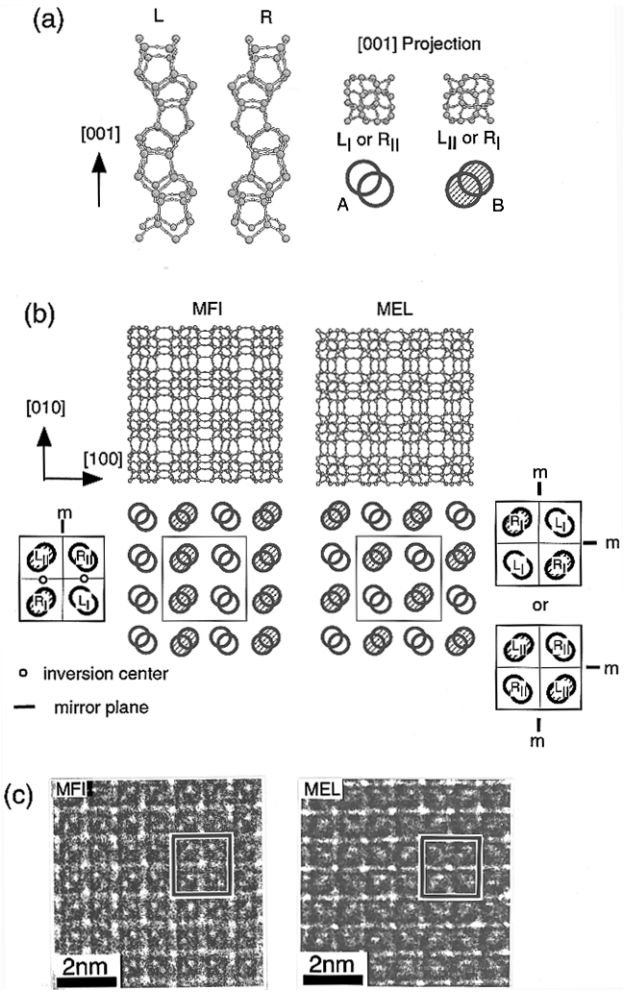

Figure 2. Schematic diagrams of (a) two types of pentasil chains and (b) MFI and MEL framework structures and unit cells (rectangles) projected along the [001] direction, represented by pentasil chains. (c) Corresponding HREM images of MFI and MEL with inserted rectangles showing the unit cell size.

images for MFI and MEL are shown in Figure 2c with inserted squares showing the unit cells. The projected structures are therefore distinguished by the arrangements of the A and B chains; that is, A and B are alternately arranged along both the [100] and [010] directions for MEL, and the alternate A and B appears along only the [100] direction for MFI.

Experimental Section

The all-silica MEL crystal was synthesized by hydrothermal treatment, and the details of the synthesis was reported.[15] The B-MEL crystal was synthesized using NaOH, $Na_2B_4O_7$, Cabosil M5, and H_2O, using seed crystal (MEL) and a template of *N*,*N*-diethyl-3,5-dimethylpiperidium hydroxide. The resulting crystal has a compositional ratio of $SiO_2/B_2O_3 = 72$.

To investigate the morphology of the MEL and B-MEL crystallites, SEM images were taken using a scanning electron microscope (S-800) operated at 2 kV without metal coating. ED and HREM observations were performed on a 1250 kV electron microscope (JEM-ARM1250) with Cs = 1.7 mm. For TEM observations, the crystallites were crushed in an agate mortar, dispersed in acetone, and placed on a holey carbon film.

Results and Discussion

1. Images and ED Patterns. Figure 3 shows SEM images of (a) MEL and (b) B-MEL crystallites, and (c) schematic drawings of the crystal shapes together with crystal axes. The MEL crystallites have a rectangular parallelepiped shape with large flat surfaces, which correspond to (100) and (010) planes. It is clear from the image that MEL crystallites show 4-fold rotational symmetry, which is consistent with the point symmetry of the MEL framework structure. The result suggests that the MEL crystallite has few faults. This was fully confirmed by HREM images, which were published.[16] The B-MEL crystallites show different morphology from that of MEL; that is, it has flat (100) and (010) surfaces, but the surfaces perpendicular to the *c*-axis are rounded and consist of many small steps on the surfaces.

Figure 4 shows ED patterns of the MEL and B-MEL crystals taken with the incident beam parallel to the [001] and [100] directions. The patterns of parts a and b of Figure 4 clearly show 4-fold rotational symmetry corresponding to the symmetry of the MEL structure projected along the [001] direction. A systematic absence of diffraction spots with $h + k + l = 2n + 1$ (n represents integers), corresponding to the extinction rule of the space group $I\bar{4}m2$ of the MEL crystal, is observed in parts a and d of Figure 4. No extra reflections can be observed in these patterns, but in the ED patterns of the B-MEL crystal, one can notice characteristic diffuse streaks along the [100] and [010] directions through the spots of $hk0$ ($h,k = 2n + 1$) in Figure 4b and around $00l$ ($l = 2n$) and $0kl$ ($k = 5n$, $l = 2n + 1$) spots in Figure 4e. Their intensity distributions are schemati-

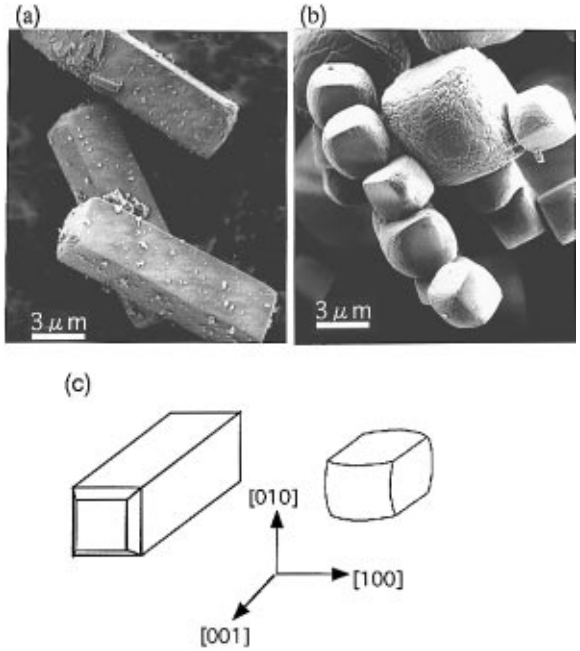

Figure 3. SEM images of (a) MEL and (b) B-MEL crystallites. (c) Schematic diagram of the crystallite's shape of MEL and B-MEL and directions of crystal axes.

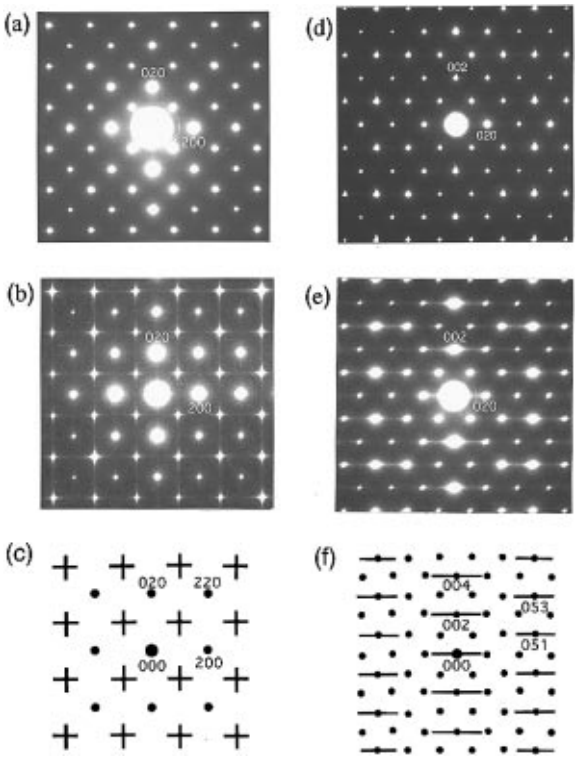

Figure 4. ED patterns taken with the incident beam parallel to the [001] direction of (a) MEL and (b) B-MEL and taken along the [100] incidence of (d) MEL and (e) B-MEL. (c) and (f) are schematic drawings of the intensity distributions of (b) and (e), respectively.

cally shown in parts c and f of Figure 4. It is confirmed that the intensity distributions of the diffuse streaks are not planar but linear and sharp.

Figure 5a shows a typical HREM image of B-MEL taken with the incident beam along the [001] direction. In the image, one can see weak modulation of bright dot arrays from an oblique viewing along the diagonal directions. From the correspondence between the bright dots in the image and the chain positions, which can be derived from a simulated HREM image and inserted models in Figure 5b, it is suggested that the

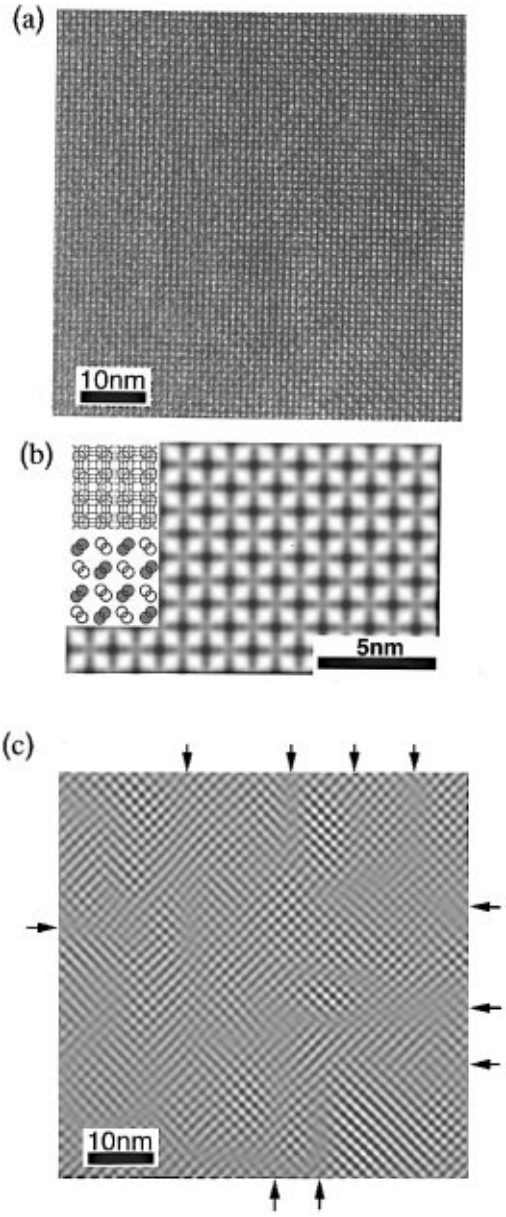

Figure 5. (a) HREM image of B-MEL taken with the incident beam along the [001] direction. (b) Simulated HREM image corresponding to (a), using the parameters with an accelerating voltage = 1250 kV, a crystal thickness = 600 Å and a defocus value = −218 Å, with a schematic diagram of the projected framework structure (inserted at the top left) and an illustration of the chain array (middle left). (c) Processed image of (a).

contrast modulation results from no modulation of chain positions but from that of chain types. To enhance the contrast modulation, an image processing of Figure 5a was carried out by a Fourier-filtering image reconstruction in which an inverse Fourier transformation was performed by using 000 and four reflections of 110 type in the Fourier diffractogram obtained from Figure 5a. Figure 5c is the reconstructed image corresponding to Figure 5a. In the processed image, one can clearly see the hazy contrasts running parallel to the (100) and (010) planes, as shown by arrows, and displacements of lattice fringes parallel to the (110) plane across the hazy contrast. The appearance of a high density of the faults parallel to (100) and (010) planes can be concluded as the cause of the streaks in the ED patterns of parts b and e of Figure 4.

2. Structure Model of the Faults. Using the A and B chains as defined above, a model of the faults in the framework structure of B-MEL projected along the [001] direction is

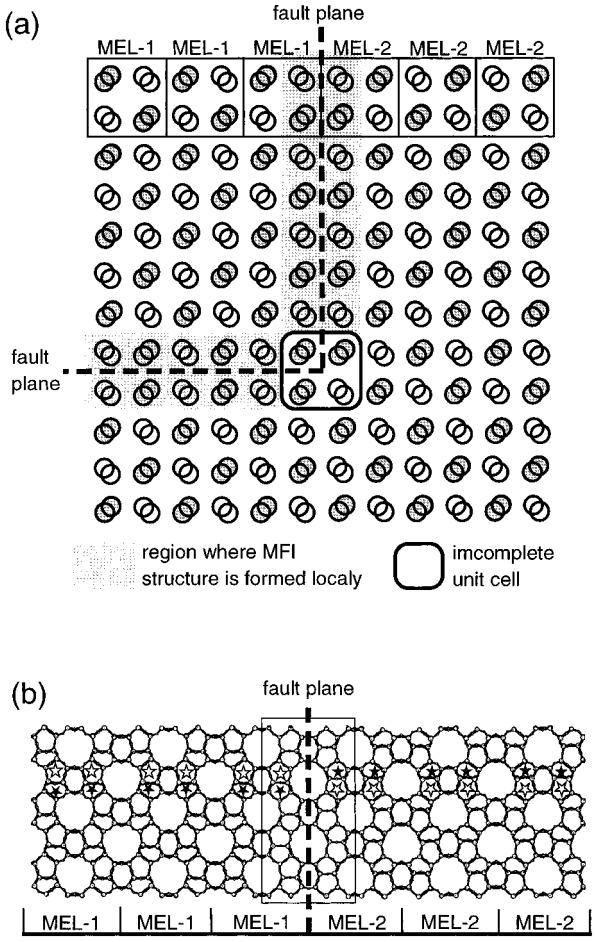

Figure 6. Schematic diagrams of the framework structure across faults projected (a) along the [001] direction, using the A and B pentasil chains, and (b) along the [100] direction. There are two different unit cells across the fault plane. The local structure within the rectangle in (b) corresponds to the MFI structure.

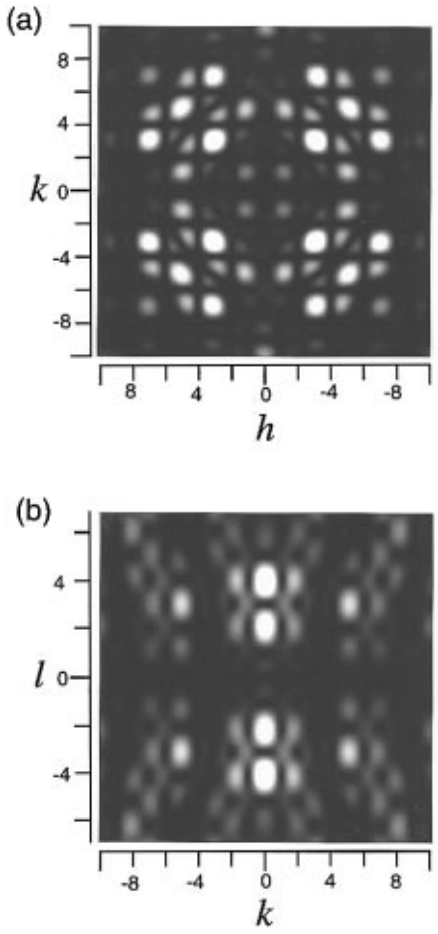

Figure 7. Calculated intensity distributions of $|F_{\mathrm{MEL}-1}(\mathbf{h}) - F_{\mathrm{MEL}-2}(\mathbf{h})|^2$ on the (hk0) reciprocal plane (a) and the (0kl) reciprocal plane (b).

schematically illustrated in Figure 6a. At the top of the figure, two different unit cells, which have the same MEL structure but different origins of the displacement vector **a**/2 or **b**/2, can be seen across the fault plane. Consequently, arrays of the A chains parallel to the [110] or [1$\bar{1}$0] directions are displaced by those of the B chains. Since an interval of the arrays of the A or B chains parallel to the [110] or [1$\bar{1}$0] directions in Figure 6a corresponds to that of lattice fringes parallel to the same directions in Figure 5c, this model can interpret characteristic features of the faults contrast in Figure 5c. A schematic diagram of the framework structure projected along the [100] direction, which is perpendicular to the viewing direction of Figure 6a, is illustrated in Figure 6b. As can be seen by white and black stars showing the positions of two different five-membered rings, one can understand the structural relationship between two domains across the fault. From this model, we can explain the steak patterns of the B-MEL, as follows.

In general, diffuse scattering intensity distribution produced by a mixture of two types of unit cells can be described by two factors: one is the factor of geometry of the boundaries that is determined by a distribution of the two types of unit cells and another is the square of the modulus of the difference between structure factors of the two types of unit cells, namely, $|F_1(\mathbf{h}) - F_2(\mathbf{h})|^2$.[17] F_1 is structure factor of the unit cell at a reciprocal point **h**, and F_2 is that of another cell . Parts a and b of Figure 7 show computed intensity distributions of $|F_{\mathrm{MEL}-1}(\mathbf{h}) - F_{\mathrm{MEL}-2}(\mathbf{h})|^2$ on the (hk0) and (0kl) reciprocal planes, respectively. Figure 7a shows that the intensity at any reciprocal point of hk0 (h,k = 2n) is zero, and the distribution of Figure 7b shows that the intensities at reciprocal points of 0kl (k = 0, l = 2n, and k = ±5, l = ±3) are strong. Combining the result of HREM showing the existence of a high density of planar faults parallel to (100) and (010) planes, which produces diffuse streaks in ED patterns, the two calculated intensity distributions of the structure model of the fault are in good agreement with the streak patterns in the observed ED patterns of Figure 4.

It is clear from Figure 6 that the MFI structure with double pentasil sheets is locally produced at the planar faults. This MFI framework can be connected to a neighboring MEL framework without the appearance of any dangling bonds except at the meeting line along [100]. Many dangling bonds must be produced in the meeting region. From our HREM experiments, we found that the B-MEL crystal is more sensitive to electron irradiation than the MEL. This observation also suggests that the B-MEL crystal has more dangling bonds than MEL.

3. Model of Growth Process of the B-MEL Crystal. By use of an arrangement of the pentasil chains, the framework structure of B-MEL including faults can be described, as shown in Figure 6a. Assuming that the chain is a growing unit on the MEL crystal, a model for the growth process on {100} surfaces of the B-MEL crystal, which include the faults, is proposed as follows. A nuclear crystallite with the same morphology as shown in the SEM image (Figure 3b) is assumed as a substrate for the growth process. First, a new chain is attached to the surface, and consequently, two steps are formed on the substrate on both sides of the chain. The next new chain will be formed at the steps because the probability of forming a new chain on the step is expected to be larger than that on flat surfaces (steps and kinks are known to be active sites in crystal growth). If

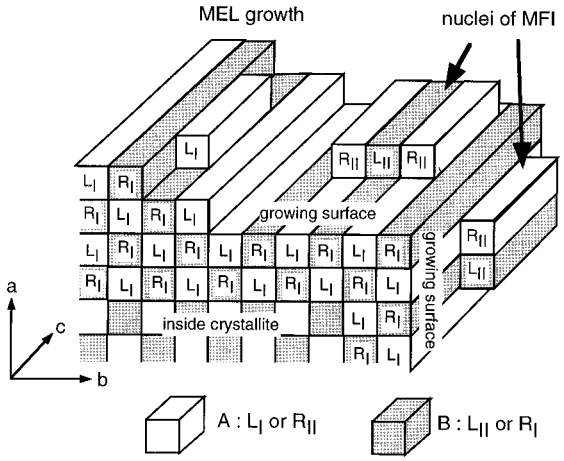

Figure 8. Schematic diagram of the model of crystal growth process in the B-MEL crystal. Top left shows the process of MEL growth. Nuclei of the MFI structure are found on top right and right sides. As these nuclei grow, an interrupted structure will form with dangling bonds.

the types of the new chain and substrate are different, the new chain produces a part of the MEL crystal (top left in Figure 8). If they are the same type, the MFI structure is constructed (top right and right side). The type of new chain is fixed by the condition of connection to another chain and substrate without dangling bonds. Following such a process, new chains are produced along the {100} surface, and consequently, the crystal grows in a thickness of the chain width. If the MFI structure is grown on the (100) and (010) surfaces of MEL, a chain with dangling bonds is produced along the meeting line (see also Figure 6a). The dangling bonds will be terminated with OH. Figure 8 is a schematic drawing of a growth process of the B-MEL crystal and shows the relations between the new chains and the substrate surfaces.

In this growth model, we speculate that the boron atoms interfere with the role of the template to stabilize the MEL nuclei/or to block the MFI on the growing surfaces, and consequently, the MFI nuclei are produced in B-MEL.

Acknowledgment. The intergrowth problem was studied by Sir John Meurig Thomas and Dr. G. R. Millward when one of the authors (O.T.) was a Visiting Research Fellow of the Royal Society (October 1982 to March 1984). O.T. is greatly indebted to Sir John Thomas for his great encouragement and discussion since then and to the Royal Society and British Council for support. CREST(JST), Grant-in-Aid, Ministry of Education, Science, Culture and Sports in Japan, and Sumitomo Chemical Corp. are greatly acknowledged for their financial supports. Y.N. acknowledges Gregory S. Lee for assistance with the synthesis.

References and Notes

(1) Kokotailo, G. T.; Lawton, S. L.; Olson, D. H.; Meier, W. M. *Nature* **1978**, *272*, 437.
(2) Kokotailo, G. T.; Chu, P.; Lawton, S. L.; Meier, W. M. *Nature* **1978**, *275*, 119.
(3) Thomas, J. M.; Audier, M.; Klinowski, J. *J. Chem. Soc., Chem. Commun.* **1981**, 1221.
(4) Thomas, J. M.; Millward, G. R. *J. Chem. Soc., Chem. Commun.* **1982**, 1380.
(5) Thomas, J. M.; Millward, G. R.; White, D.; Ramdas, S. *J. Chem. Soc., Chem. Commun.* **1988**, 434.
(6) Millward, G. R.; Ramdas, S.; Thomas, J. M.; Barlow, M. T. *J. Chem. Soc., Faraday Trans. 2* **1983**, *79*, 1075.
(7) Terasaki, O.; Thomas, J. M.; Millward, G. R.; Watanabe, D. *Chem. Mater.* **1989**, *1*, 158.
(8) Foger, K.; Sanders, J. V.; Seddon, D. *Zeolites* **1984**, *4*, 337.
(9) Scholle, K. F. M. G. J.; Kentgens, A. P. M.; Veeman, w. S.; Frenken, P.; van der Velden, G. P. M. *J. Phys. Chem.* **1984**, *88*, 5.
(10) Chu, C. T.-W.; Chang, C. D. *J. Phys. Chem.* **1985**, *89*, 1569.
(11) Liu, X.; Klinowski, J. *J. Phys. Chem.* **1992**, *96*, 805.
(12) Stave, M. S.; Nicholas, H. B. *J. Phys. Chem.* **1995**, *99*, 15046.
(13) Perego, G.; Cesari, M.; Allegra, G. *J. Appl. Crystallogr.* **1984**, *17*, 403.
(14) Terasaki, O.; Ohsuna, T. *Catal. Today* **1995**, *23*, 201.
(15) Nakagawa, Y. WO Patent 95 09812, 1995.
(16) Terasaki, O.; Ohsuna, T.; Sakuma, H.; Watanabe, D.; Nakagawa, Y.; Medrud, R. *Chem. Mater.* **1996**, *8* (2), 463.
(17) Cowley, J. M. *J. Appl. Phys.* **1950**, *21*, 24.